LANGMUIR Article
Cite This: Langmuir 2017, 33, 12155-12170
pubs.acs.org/Langmuir

Mechanisms and Control of Self-Emulsification upon Freezing and Melting of Dispersed Alkane Drops

Zhulieta Valkova,[†] Diana Cholakova,[†] Slavka Tcholakova,[†] Nikolai Denkov,[†] and Stoyan K. Smoukov*[,†,‡,§]

[†]Department of Chemical and Pharmaceutical Engineering, Faculty of Chemistry and Pharmacy, Sofia University, 1 James Bourchier Avenue, 1164 Sofia, Bulgaria

[‡]Active and Intelligent Materials Laboratory, School of Engineering and Materials Science, Queen Mary University of London, Mile End Road, London E1 4NS, U.K.

[§]Active and Intelligent Materials Laboratory, Department of Materials Science & Metallurgy, University of Cambridge, 27 Charles Babbage Road, Cambridge CB3 OFS, U.K.

Supporting Information

ABSTRACT: Emulsification requires drop breakage and creation of a large interfacial area between immiscible liquid phases. Usually, high-shear or high-pressure emulsification devices that generate heat and increase the emulsion temperature are used to obtain emulsions with micrometer and submicrometer droplets. Recently, we reported a new, efficient procedure of self-emulsification (Tcholakova et al. *Nat. Commun.* **2017**, *8*, 15012), which consists of one to several cycles of freezing and melting of predispersed alkane drops in a coarse oil-in-water emulsion. Within these freeze–thaw cycles of the dispersed drops, the latter burst spontaneously into hundreds and thousands of smaller droplets without using any mechanical agitation. Here, we clarify the main factors and mechanisms, which drive this self-emulsification process, by exploring systematically the effects of the oil and surfactant types, the cooling rate, and the initial drop size. We show that the typical size of the droplets, generated by this method, is controlled by the size of the structural domains formed in the cooling–freezing stage of the procedure. Depending on the leading mechanism, these could be the diameter of the fibers formed upon drop self-shaping or the size of the crystal domains formed at the moment of drop-freezing. Generally, surfactant tails that are 0–2 carbon atoms longer than the oil molecules are most appropriate to observe efficient self-emulsification. The specific requirements for the realization of different mechanisms are clarified and discussed. The relative efficiencies of the three different mechanisms, as a function of the droplet size and cooling procedure, are compared in controlled experiments to provide guidance for understanding and further optimization and scale-up of this self-emulsification process.

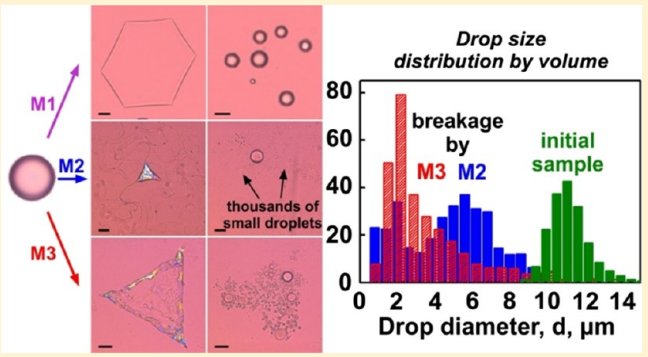

INTRODUCTION

Many common industrial and consumer products, including paints, shampoos, lotions, cosmetic creams, salad dressings, mayonnaise, and some pharmaceutical formulations, are emulsions (liquid-in-liquid dispersions). Therefore, emulsification processes are widely used in various chemical, pharmaceutical, agro, food, and cosmetic technologies.[1−3]

The emulsification is typically performed with high-shear or high-pressure devices, which generate sufficiently high viscous or inertial hydrodynamic stresses and are able to deform and disrupt the emulsion drops into the desired micrometer and submicrometer sizes.[1−7] The energy dissipated in the classical emulsification devices is several orders of magnitude higher than the interfacial energy of the small droplets generated.[1−3] Thus, emulsification is an energy-intensive process with most of the energy wasted into heat. Furthermore, the dissipated energy may increase the temperature of the processed emulsion by dozens of degrees, which might have a deteriorating effect on technological emulsions containing temperature-sensitive components, such as bioactive molecules, in pharma, cosmetic, and agro applications.[1−3]

Several techniques have been explored to address the need to handle temperature-sensitive formulations. Membrane emulsification enables low-temperature emulsification at the expense of lower productivity and limited drop size range, which does not include the submicrometer domain.[8,9] As a result of these limitations, membrane emulsification, though being highly

Received: June 15, 2017
Revised: August 13, 2017
Published: October 8, 2017

DOI: 10.1021/acs.langmuir.7b02048
Langmuir 2017, 33, 12155−12170

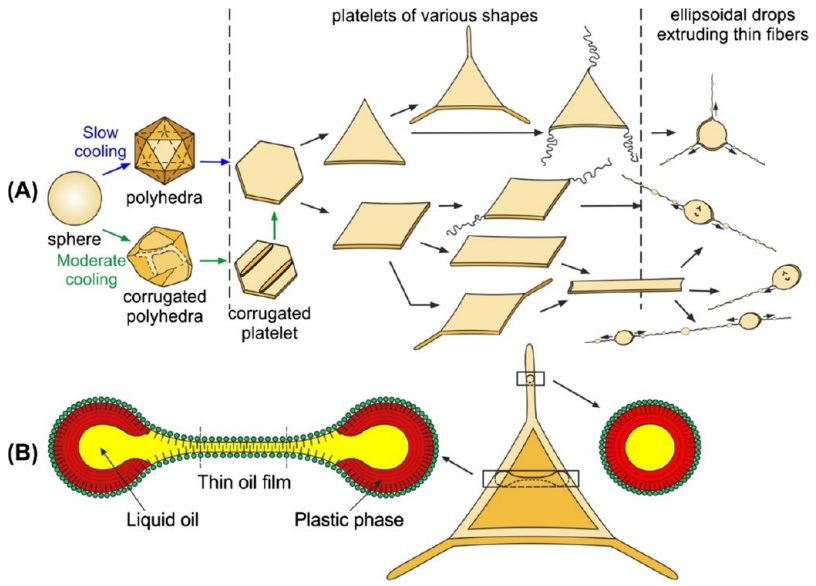

Figure 1. (A) Drop-shape evolutionary scheme, showing the main stages through which the oily drops pass upon cooling. (B) Schematic presentation of the mechanism causing drop-shape transformations; for more details, see refs 23−25 and 34.

energy efficient, has found a limited application outside the research labs.

Several other techniques based on spontaneous drop fragmentation (self-emulsification) were proposed for the generation of micrometer and submicrometer droplets.[10−21] Some of these techniques are based on the reduction of the oil solubility in a continuous medium, which could be either a mixture of solvents or a surfactant-based microemulsion.[19−21] By changing the solvent composition and/or temperature, one could reduce the oil solubility and thus generate tiny droplets of nanometer size. These methods require rather high solubility or solubilization of oil in the continuous medium to generate emulsions of reasonably high drop volume fraction. Therefore, either polar oils with relatively small molecules (in the case of solvent precipitation) or rather high surfactant concentrations (in the case of microemulsions) are needed to apply this approach.

Another class of self-emulsification methods utilizes changes in the solvent composition, surfactant composition, or temperature to inverse an initially water-in-oil into oil-in-water emulsion or vice versa.[12,13] Small droplets may be formed in this phase-inversion process, although important elements in the underlying mechanisms of drop fragmentation are still unclear. Usually, the phase-inversion techniques are explained with the change in the spontaneous curvature of the interfacial surfactant layer, so that the preferred enclosed phase changes from oil to water or vice versa. These techniques also require surfactants of relatively high concentrations, and this requirement creates problems for many potentially useful applications.

Self-emulsification could be induced also by mass transfer between the oil and water phases of properly balanced surfactants, such as AOT (dioctyl sulfosuccinate sodium salt) or surfactant + cosurfactant mixtures, which have solubility in both bulk phases.[14−16] Several complex mechanisms, related to the transfer of surfactants across the interface (e.g., interfacial turbulence induced by the Marangoni effect or ultralow interfacial tension) and to the effect of oil solubilization on the morphology of surfactant aggregates (e.g., spontaneous bursting of the vesicles after oil solubilization) were shown to induce spontaneous formation of micrometer and submicrometer emulsion droplets.[15,16]

All these methods of self-emulsification have their specific limitations. Therefore, other low-temperature and low-energy emulsification processes with high productivity are needed to advance our current technologies.

Recently, we demonstrated a novel low-energy and low-temperature self-emulsification process, in which the oil droplets in an oil-in-water emulsion break up spontaneously into much smaller droplets in the course of temperature cycling around the freezing temperature of the oil drops. The typical temperature cycle includes slow cooling, freezing of the drops, and their remelting. The repeat of these cycles leads, under appropriate conditions, to the formation of droplets with a submicrometer diameter. Optical microscopy observations showed that this self-emulsification technique involves three nontrivial mechanisms of drop-bursting.[22]

In the current study, we present each of the newly discovered mechanisms in more detail and clarify systematically the effect of the main factors, viz., the alkane and surfactant types, cooling rate, and initial drop size, on each of these mechanisms and on the overall self-emulsification process.

Hereafter, we explain briefly the shape transformations observed during the cooling stage of the temperature cycling (before the drop-breakup or complete drop-freezing) because these transformations are intimately related to the self-emulsification mechanisms discussed in the current paper. In our recent studies,[23−25] we showed that micrometer emulsion drops from alkanes, alkenes, alcohols, triglycerides, asymmetric alkanes, mixtures of these compounds, and even mixtures of some commercial oils (e.g., cocoa butter, lard, and coconut oil) with a small amount of linear alkane, ca. 15 vol % or higher, can self-shape upon cooling when long-chain surfactants are used as the emulsion stabilizer (see Figure 1A). The long-chain surfactant forms adsorption layers on the drop surface, which freeze upon cooling before the freezing of the oil in the drop interior.[23,24,26] In this way, the frozen adsorption layer creates a surface template for the formation of the so-called "plastic rotator phase" beneath the drop surface (Figure 1B). The molecules in such a plastic phase have a long-range translational order and

DOI: 10.1021/acs.langmuir.7b02048
Langmuir 2017, 33, 12155−12170

some rotational freedom along their long axes. The plastic rotator phases have been known[27−33] for years to appear as an intermediate between the isotropic liquid and the fully frozen crystal phase of the cooled alkanes.

The plastic phases possess certain elasto-plastic mechanical strength. Therefore, the appearance of a plastic phase on the drop surface leads to deformation of the emulsion drops. The optical observations show that the drops deform first into polyhedrons, which rapidly flatten to form hexagonal, tetragonal, or trigonal platelets. This sequence of shape transformations was explained with the formation of an expanding frame of cylindrical rods of the plastic phase at the drop periphery. The partial mobility of the molecules assembled in the rotator phase allows for molecular exchange and dynamic equilibrium with the neighboring liquid alkane. As a result, the plastic frame expands and reshapes with time, "sucking" molecules from the liquid interior of the platelet and thus "pushing" the oil−water interface, forming various geometric shapes, as shown in Figure 1A. A theoretical model was developed around these ideas, which explained the observed platelet shape sequence and the growth of asperities from the acute corner angles of the triangle and tetragonal platelets, in agreement with the experiment.[34] Eventually, the platelets may undergo a kind of capillary instability, forming ellipsoidal drops that extrude thin and very long fibers. Depending on the specific oil−surfactant pair and the cooling protocol, the droplets may freeze completely into solid particles in any of these shapes. In addition, the drops may break into smaller droplets during cooling or upon melting.

The paper is organized in the following way. In the Experimental Section, we describe the materials and methods used. In the Results and Discussion section, first we describe each of the mechanisms of self-emulsification and how these mechanisms respond to changes in alkane, surfactant, drop size, and cooling rate. Finally, we compare the effectiveness of these mechanisms and discuss how one could control the different factors to obtain an emulsion with a desired drop size distribution.

EXPERIMENTAL SECTION

Materials. Linear alkanes with different chain lengths were used as the dispersed oily phase in the studied emulsions. Tetradecane (referred to as C_{14}), pentadecane (C_{15}), hexadecane (C_{16}), heptadecane (C_{17}), octadecane (C_{18}), nonadecane (C_{19}), and eicosane (C_{20}) were all products of Sigma-Aldrich with purity >99%. Their melting temperatures, T_m, vary between 5.5 °C for C_{14} and 37 °C for C_{20}. Detailed information on the physical properties of these alkanes is presented in the Supporting Information Table S1. All alkanes were used as received, without further purification.

To stabilize the emulsions, we used a variety of nonionic and ionic surfactants. The nonionic surfactants were from two main groups—polyoxyethylene alkyl ethers (C_nEO_m) and polyoxyethylene sorbitan monoalkylates ($C_nSorbEO_{20}$), which differ in the length of their alkyl chain, n, which varied between 12 and 22 and in the number of oxyethylene units, m, which varied between 2 and 50. The $C_{16}EO_2$ surfactant is the only oil-soluble surfactant used, whereas the others are water-soluble surfactants. We also used three ionic surfactants—the cationic surfactants cetyltrimethylammonium bromide ($C_{16}TAB$) and octadecyltrimethylammonium bromide ($C_{18}TAB$) and the anionic sodium octadecyl sulfate ($C_{18}SO_4Na$). Detailed information on the purity, hydrophilic−lipophilic balance values of the nonionic surfactants, and the surfactant producers is presented in the Supporting Information Table S2. All surfactants were used as received.

For emulsion preparation, the emulsifier concentration in the aqueous solutions (1.5 wt % for all nonionic surfactants, 0.37 wt % for the anionic surfactant, and 0.5 wt % for the cationic surfactants) was chosen to be sufficiently high as to suppress completely the drop−drop coalescence during the emulsion preparation and to avoid significant surfactant depletion during the experiments (due to adsorption on the increasing surface of the deforming drops).

All aqueous solutions were prepared with deionized water, which was purified by an Elix 3 module (Millipore, USA).

Methods. *Preparation of the Initial Emulsions.* The initial alkane-in-water emulsions were prepared by a laboratory microkit membrane emulsification module from Shirasu Porous Glass Technology (SPG, Miyazaki, Japan). The oil phase was passed through tubular glass membranes with an outer diameter of 10 mm and a working area of approximately 3 cm^2. This method allows production of drops with a relatively narrow drop size distribution.[8,9,35−38] Membranes with a mean pore diameter of 2, 3, 5, and 10 μm were used for preparing the initial emulsions with drop diameters around 6, 11, 17, and 34 μm.

When preparing emulsions with substances that are solid at room temperature, we melted them by heating before emulsification and maintained sufficiently high temperature in the laboratory to avoid the liquid−solid phase transition before the actual emulsification experiments.

Microscope Observations of the Freeze−Thaw Cycles. All observations were performed with an Axioplan or Axio Imager M2m optical microscope (Zeiss, Germany). For the freeze−thaw cycles, we used transmitted, cross-polarized white light with included λ (compensator) plate, situated after the sample and before the analyzer, at 45° with respect to both the analyzer and the polarizer. Under these conditions, the liquid background and the fluid objects have a typical magenta color, whereas the birefringent areas appear brighter and may have intense colors.[39,40] When taking images for the determination of the drop size distribution, we used transmitted light. Long-focus objectives 20×, 50×, and 100× were used.

A specimen of the studied emulsion was placed in a capillary with a rectangular cross-section: 50 mm length, 1 mm width, and 0.1 mm height. The capillary was enclosed within a custom-made metal cooling chamber with optical windows for microscope observation. The chamber temperature was controlled by a cryo-thermostat (JULABO CF30, Cryo-Compact Circulator) and measured close to the emulsion location, using a calibrated thermocouple probe with an accuracy of ±0.2 °C (Supporting Information Figure S1). The thermoprobe was inserted in one of the orifices of the aluminum thermostatic chamber and mounted in a position where a capillary with the emulsion sample would be normally placed for microscope observations. In the neighboring orifice, the actual capillary with the emulsion sample was placed. The correct measurement of the temperature was ensured by calibrating the thermocouple with a precise mercury thermometer in the respective range of temperatures measured. Furthermore, we always observe melting of the frozen particles at temperatures very close to T_m ± 0.2 °C, where T_m is the melting temperature of the bulk oil, reported in the literature.

The freeze−thaw (F/T) experiments of the dispersed drops were performed as follows:

(1) The cooling process started at a temperature at least 5° higher than the bulk melting temperature of the studied alkane (see Table S1). The samples were cooled at a fixed cooling rate and varied in different experiments (usually between 0.15 and 1.5 K/min). The temperature in the system was lowered until a complete freezing of the dispersed oil drops was observed. Note that only the dispersed phase underwent phase transitions during our experiments and solidified; the continuous medium (aqueous surfactant solution) always remained liquid.

(2) The drop-melting process was performed at a fixed heating rate and varied between 0.1 and 10 K/min. The temperature in the system was increased until reaching the initial temperature at which all dispersed entities were in a liquid state.

Procedures (1) and (2) may be repeated with the same sample to accomplish several consecutive F/T cycles.

Determination of Drop Size Distribution in the Emulsions. The drop size distribution in emulsions was determined from microscope images taken after each F/T cycle with 50× and 100× objectives. The

DOI: 10.1021/acs.langmuir.7b02048
Langmuir 2017, 33, 12155−12170

accuracy in the measurements of the drop diameter by this method is ±0.3 μm.[41] Drop diameters were measured one by one using custom-made image analysis software. The diameters of more than 1000 droplets in each sample were measured.

The mean volume−surface diameter was determined from the relation $d_{32} = \sum_i N_i d_i^3 / \sum_i N_i d_i^2$, where N_i is the number of drops with diameter d_i. The maximal diameter by number, d_{N95}, denotes the diameter that separates the size distribution by number so that 95% of the drops are smaller, whereas the other 5% are bigger than d_{N95}. Similarly, the maximal diameter by volume, d_{V95}, presents the diameter of drops for which 95% of the whole dispersed oil in the sample is included in drops with diameter smaller than d_{V95}. Analogously, the mean diameters by number and by volume, d_{N50} and d_{V50}, denote the diameters that divide 50% of the drops to be below and above the respective diameter.

Interfacial Tension Measurements. The alkane−water interfacial tension, γ, was measured by the drop-shape analysis at different temperatures.[42,43] The shape of millimeter-sized pendant oil drops immersed in the surfactant solution was recorded and analyzed by the Laplace equation of capillarity (instrument DSA100 by Krüss, Germany). The thermostatic cell TC40 was used to vary the temperature of the measured system with a precision of ±0.2 °C. All reported results were measured before the detection of any sign of freezing of the adsorption layer on the pendant drop surface. Such a sign is the abrupt increase of the fit error in the description of the surface of the pendant drop by Laplace equation (see, e.g., the explanations in refs 23 and 44).

In a typical experiment, the temperature was decreased with a rate mimicking that in the actual experiments with slowly cooled emulsions (between 0.1 and 0.5 K/min). In separate experiments, the actual temperature at the position of the pendant drop was measured by a calibrated thermocouple. Also, for some of the systems, a discrete set of decreasing temperatures was used with an equilibration of 15 or 60 min at each temperature. For a given temperature, the interfacial tensions measured at a constant cooling rate and at a fixed temperature were in agreement, with the tension measured at a constant temperature being the same or only slightly lower (within 0.5 mN/m) as a very slow rearrangement of the molecules may take place in the frozen adsorption layers. The latter difference was observed at the lowest temperatures only, whereas the deformation of the emulsified drop in the same solution had already started at higher temperatures.

These different regimes of cooling were used to check for possible effects of the finite time required for the temperature at the drop center to equilibrate. One can estimate this time from the laws of heat-diffusion in a spherical body.[45] These estimates show that the relaxation of the temperature difference from the surface to the center of spherical drops with a diameter of 40 μm, like the bigger drops present in the studied emulsions, occurs for around 5 ms

$$\tau \approx \frac{d^2}{4\chi} = \frac{(40\ \mu\text{m})^2}{3.2 \times 10^{-7}} = 5\ \text{ms}$$

Here $\chi = (\kappa/\rho C_p)$ is the thermal diffusivity of the dispersed phase, κ, ρ, and C_p are its thermal conductivity, mass density, and heat capacity, respectively. For the millimeter size pendant drops used to measure the oil−water interfacial tension, this relaxation time is of the order of several seconds.

As clarified from the obtained experimental results and from the above estimates, the cooling rates were sufficiently low to avoid complications related to possible difference in the temperatures on the surface and in the body of the studied drops. As the experiments at a constant cooling rate mimic better the actual experiments with cooled emulsions, we show these data for the interfacial tension in Figure 8 below.

RESULTS AND DISCUSSION

In this section, we present our experimental results about the self-emulsification phenomena and discuss the effects of the main factors: alkane chain length, surfactant type, initial drop size, and cooling rate. First, we describe the process of drop-bursting observed upon emulsion cooling (Mechanism 1). Then we discuss the two mechanisms observed upon emulsion heating—capillary instability of the melting fibers (Mechanism 2) and melt−crystal fragmentation of the platelets (Mechanism 3). Next, we compare the effectiveness of the different mechanisms, and on this basis, we discuss the results obtained with various systems and the possible approaches for control of the drop size distribution.

Droplets Bursting upon Cooling (Mechanism 1). Oil-in-water emulsion drops stabilized by appropriate surfactants spontaneously change their shape upon cooling, as described in the Introduction. An additional process is observed in some of the emulsions, namely drop-bursting into smaller drops, as shown in Figure 2. In this process, a single emulsion drop

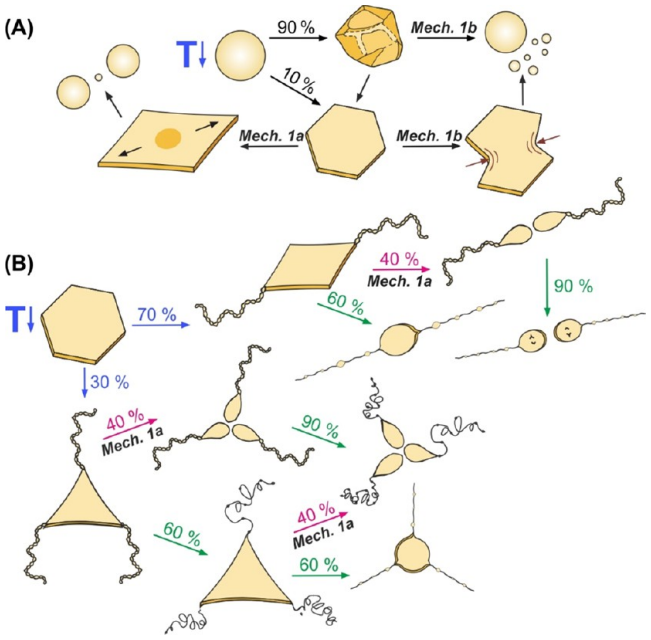

Figure 2. Scheme of drop-shape evolution, including the possible drop-bursting processes upon cooling. Emulsion drops stabilized by long-chain surfactants spontaneously change their shape upon cooling. Along this drop-shape evolution, bursting processes may be observed in which 2 to more than 10 "daughter" droplets are formed. (A) Upon cooling, the spherical drops deform into polyhedrons and then into platelets. Depending on the specific systems and conditions, the platelets may deform and break symmetrically because of the formation of a thin oil film in the platelet center (Mechanism 1a, see also Figure 3) or may break asymmetrically because of surface corrugations and local platelet thinning around the platelet periphery (Mechanism 1b, see also Figure 4). This stage often occurs several times as droplets breakup to smaller and smaller sizes, before proceeding to the subsequent shapes in the evolutionary scheme. (B) Typical evolution for cooled C_{17} drops with an initial drop diameter, $d_{ini} \approx 34$ μm, stabilized by $C_{18}EO_{20}$. Arrows in blue show the deformation processes, arrows in green show the process of capillary instability, and arrows in purple show the drop-bursting processes (see text for further explanations).

spontaneously breaks into several (between 2 and 15) daughter droplets. Drop-bursting can be observed in all evolutionary stages in which the drop acquires a platelet shape. This excludes the last stages of the evolutionary scheme, in which the drops undergo shape transition to become ellipsoidal and extrude thin fibers as well as the "rodlike" stage, in which cylindrical rods with uniform thicknesses are formed, cf. Figure 1. After drop-bursting,

DOI: 10.1021/acs.langmuir.7b02048
Langmuir 2017, 33, 12155−12170

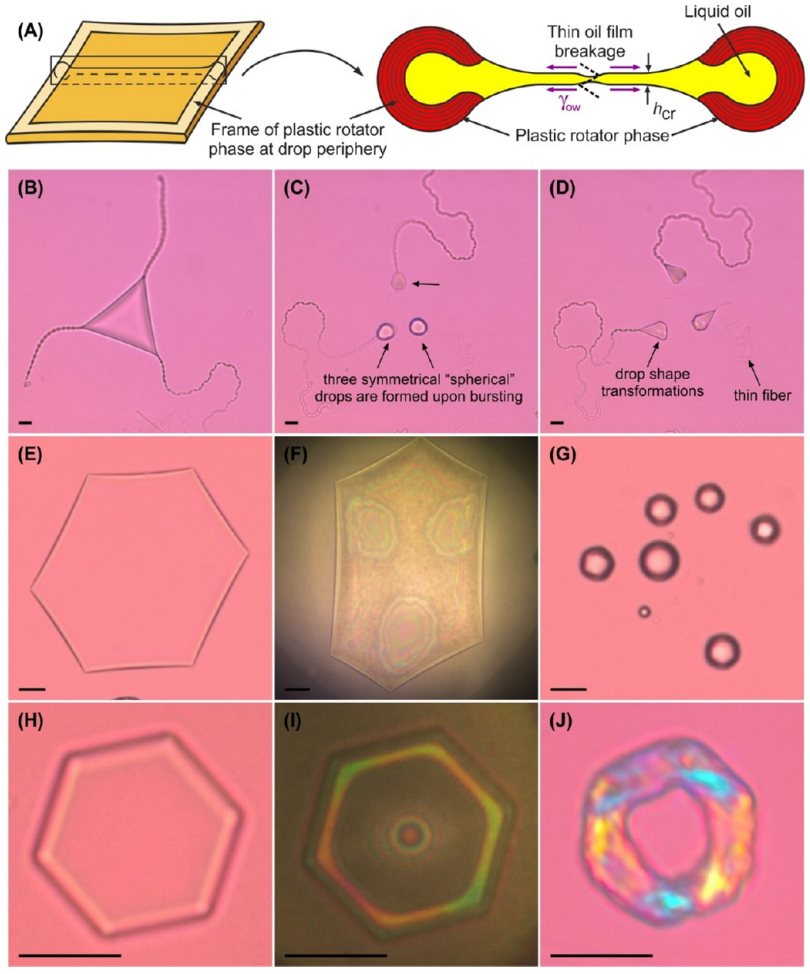

Figure 3. Drop-bursting upon cooling via platelet puncture (Mechanism 1a). (A) The cooled platelets may acquire the thinnest central region (thin water−oil−water film), which is unstable and breaks. The formed toroidal drop is capillary unstable and bursts into several smaller drops. (B−D) Microscope images of a triangular platelet with protrusions, which breaks in its center. (B) Platelet before bursting. (C) Three symmetrical daughter drops are formed after bursting, which immediately (D) start to change their shape. (E−G) Hexagonal platelet which breaks in its center observed in (E) transmitted polarized light and (F) reflected light; (G) daughter drops formed after platelet breakage. (H−J) Microscope images of a hexagonal platelet with a thin water−oil−water film in its center, observed in (H) transmitted polarized light, (I) reflected light (the thin oil film is seen in the platelet center), and (J) transmitted polarized light after freezing (a hole in the platelet center is formed due to the film breakage upon freezing). The scale bar is 10 μm. Experiments are performed with C_{16} oil drops stabilized by $C_{18}EO_{20}$ (B−G) or $C_{16}EO_2$ (H−J) surfactant.

the newly formed drops start to change their shape again, and another bursting event can be observed. To quantify this bursting sequence, we count the number of consecutive bursting events of the biggest "daughter" drops formed after each breakage event.

Two distinct versions of this mechanism are observed and described separately for the first time in the current study as the effects of various experimental factors and the final outcome of the bursting process are different.

Mechanism 1a—Drop-Bursting via Platelet Central Puncturing. This mechanism was first described in our previous paper.[22] Briefly, upon cooling, the platelet expands in area with time because the frame of the rotator phase gradually "sucks" molecules from the liquid interior of the platelet. Because the volume of the platelet is fixed, the platelet may eventually become the thinnest in its central region, as shown in Figures 1B and 3A. Thus, a thin water−oil−water film is formed in the platelet central region (Figure 3F,I), which is unstable for some surfactant−alkane pairs and punctures. The platelet puncture leads to the formation of a toroidal shape drop, which is capillary unstable and instantly breaks into several daughter droplets.

This bursting mechanism requires the formation of a platelet, which retains its shape for a sufficiently long time to thin and form an unstable water−oil−water film in its central region. This mechanism can be observed at any of the platelet stages of drop evolution—with hexagonal, tetragonal, or trigonal platelets. The platelets extruding fibers can also burst, as shown in Figure 3B−D.

Depending on the platelet shape, two (from tetragonal platelets) to six (from hexagonal platelets, Figure 3G) daughter droplets with comparable diameters are formed. The newly formed droplets have diameters between $0.5d_{ini}$ and $0.8d_{ini}$, where d_{ini} is the diameter of the initial spherical drop before its bursting. This mechanism is very effective for decreasing the size of the biggest droplets in the emulsion, characterized by d_{V95} and d_{32}. On the other hand, this mechanism is ineffective for decreasing d_{N95} and d_{N50} because very limited number of much smaller droplets (most often none, sometimes one or two) with diameter $d \leq 0.1d_{ini}$ are formed.

Mechanism 1b—Drop-Bursting Due To Breakage of the Platelet Plastic Frame. The second mechanism of drop-bursting upon cooling is again caused by platelet puncture. However, in

DOI: 10.1021/acs.langmuir.7b02048
Langmuir 2017, 33, 12155−12170

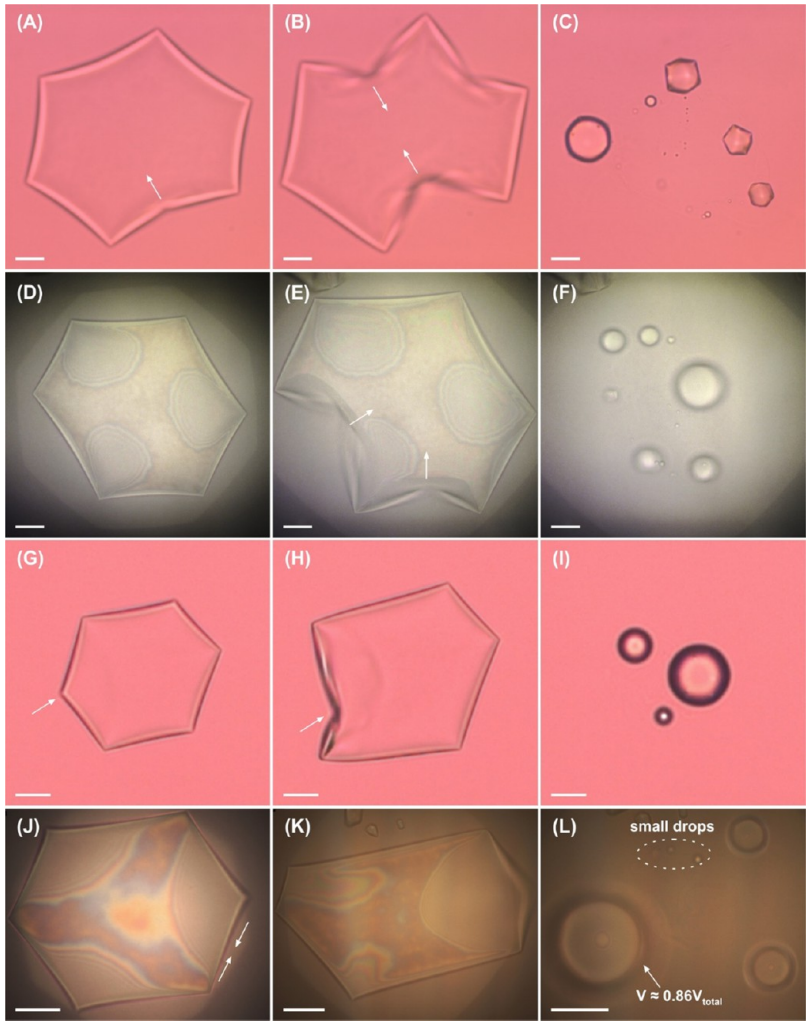

Figure 4. Drop-bursting upon cooling via rotator phase breakage and puncturing (Mechanism 1b). (A–F) Upon cooling, platelets that thin symmetrically may exhibit breakage of the rotator phase frame (B,E). As a result, the oil film thins locally and breaks (C,F). (G–L) Platelets may thin asymmetrically, and breakage of the rotator phase near the platelet tip may occur, resulting in platelet puncturing. All experiments are performed with C_{16} drops stabilized by the $C_{18}EO_{20}$ surfactant. Pictures in (A–C) and (G–I) are made in transmitted polarized light, whereas those in (D–F) and (J–L) are made in reflected white light. The scale bar is 20 μm.

this case, it is triggered by mechanical breakage of one or several of the rods from the expanding plastic frame at the drop perimeter, which on its turn leads to local thinning and rupture of the platelet near the broken plastic rod.

In our previous study, we showed that depending on the particular oil–surfactant combination used, the thickness and strength of the plastic rods of the rotator phase formed at the drop perimeter are different.[24] For example, we found that C_{16} drops stabilized by $C_{18}EO_{20}$ form a thinner and more flexible rotator phase, as compared to those stabilized by $C_{18}SorbEO_{20}$. Our observations showed that these rods of the thinner rotator phase might not be strong enough to withstand the stress created by the oil–water interfacial tension, which compresses the frame toward the platelet center. As a result, the frame of plastic rods may break, as shown in Figure 4. After such breakage, the broken rod bends toward the platelet center under the action of the interfacial tension (Figure 4B), the oil film gets corrugated locally around the broken rod, and a platelet breakage can occur via puncture at some thin local spot in the corrugated region (Figure 4C).

Another type of mechanical instability of the plastic frame and subsequent platelet breakage was also observed. It occurs close to one of the platelet vertices. The two sides forming a vertex start to bend toward the platelet center, again creating local corrugations of the platelet surfaces, followed by platelet puncturing and bursting close to the vertex (see Figure 4G–I). Mechanism 1b occurs more often via such vertex breakage event in the process of polyhedrons flattening into a platelet.

Mechanism 1b may be observed also in the process of transformation of the polyhedrons into platelets via wrinkle formation (see the lower branch in Figure 1A). When the cooling rate is higher than 1 K/min, irregular polyhedrons are formed in the initial stage of drop evolution in many of the emulsions studied. These wrinkles consume a large fraction of the oil inside the drops, and their dynamics creates mechanical stresses in the deformed drops. Drop-bursting via puncturing of the flattened regions between the wrinkles in the deformed drops may occur in this stage of drop evolution as well (see Movie S1).

The newly formed daughter drops are in much larger number when they are formed via Mechanism 1b, as compared to Mechanism 1a. Often more than 10 droplets are formed in Mechanism 1b, whereas this number is usually between 2 and 6 in Mechanism 1a. On the other hand, because the drop breakage is asymmetric in Mechanism 1b, the newly formed droplets are

DOI: 10.1021/acs.langmuir.7b02048
Langmuir 2017, 33, 12155–12170

Table 1. Frequency of Occurrence of the Different Mechanisms for the four Main Nonionic Surfactants Studied in Combination with Alkanes of Different Chain Lengths[a]

		drop-bursting upon cooling		disintegration of thin fibers		melt−crystal fragmentation
surfactant	alkane	Mechanism 1a	Mechanism 1b	Mechanism 2a	Mechanism 2b	Mechanism 3
$C_{16}EO_{20}$	C_{14}	−	−	+	+++	−
	C_{15}	−	−	++	+++	−
	C_{16}	−	−	+++	++	+
	C_{17} and longer	−	−	−	−	−
$C_{18}EO_{20}$	C_{14}	−	+	−	+++	−
	C_{15}	−	+	+	+++	+
	C_{16}	+	++	++	+++	+++
	C_{17}	+++	+++	+++	+++	+++
	C_{18}	+	+	−	−	+++
	C_{19}	−	−	−	−	++
	C_{20} and longer	−	−	−	−	−
$C_{16}SorbEO_{20}$	C_{14}	+	+++	+++	+++	−
	C_{15}	+++	+	++	+++	+++
	C_{16}	−	+	−	−	+
	C_{17} and longer	−	−	−	−	−
$C_{18}SorbEO_{20}$	C_{14}	−	+	++	++	−
	C_{15}	+	−	++	+++	+
	C_{16}	−	+	−	−	+
	C_{17} and longer	−	−	−	−	−

[a]The sign "−" denotes that the respective mechanism is not observed with this system. Plus signs denote the frequency and/or intensity of observation. One "+" sign denotes that this mechanism is observed for less than 50% of the drops and/or the mechanism is not very effective. Two "++" signs denote that the mechanism is observed for more than 80% of the drops, and the triple "+++" sign denotes that the mechanism is observed for all drops. In addition, for Mechanism 1, "+" sign denotes up to three consecutive breakage events, "++" sign denotes up to six consecutive breakage events, and "+++" sign denotes more than six consecutive breakage events. See the text for detailed explanations about the different mechanisms.

polydisperse. Usually, one or two big drops are formed, containing more than 90% of the oil volume, whereas the other formed drops are much smaller. Therefore, this mechanism is not so effective in reducing d_{32}, but it is more effective than Mechanism 1a for reducing d_{N95} and d_{N50} because of the formation of numerous small droplets.

Let us discuss now the effects of the alkane chain length, surfactant type, initial drop size, and cooling rate on this mechanism.

Effect of Alkane Chain Length on Drop-Bursting upon Cooling. In our previous study, we found that one of the most efficient surfactants for self-emulsification is $C_{18}EO_{20}$.[22] Therefore, first we discuss the behavior of drops from different alkanes (chain length varied between 14 and 20 C atoms) with the same initial drop size, $d_{ini} \approx 34\ \mu m$, stabilized by $C_{18}EO_{20}$ and cooled at 0.2 K/min.

For the longest chain length alkanes studied, nonadecane and eicosane (C_{19} and C_{20}), bursting events are not observed upon cooling, as seen from the results summarized in Table 1. The drops evolve up to the platelet stage (Figure 5A−C), but without platelet bursting being observed.

When the same experiment is performed with a shorter alkane, C_{18}, the drop transformations are easier and some breakage events (between 0 and 2) are observed via both Mechanisms 1a and 1b.

The maximal number of breakage events for the $C_{18}EO_{20}$ surfactant is observed when alkanes with a slightly shorter chain length, C_{17} and C_{16}, are used. For these alkanes, the drop-shape transformations are quite easy; the formed plastic rods are thin and fragile, and as a result, they break easily. Between 1 and more than 10 consecutive breakage events are observed for a single drop in these systems. Although the behavior of C_{16} and C_{17} drops is qualitatively similar, the number of bursting events for C_{17} is larger (typically 7 or 8, up to more than 15) as compared to those with C_{16} (typically, one to several). This difference can be explained with the preferred shape of the deformed droplets—the C_{17} drops become very flat hexagonal platelets before they pass into the next stages of the evolutionary scheme, whereas the C_{16} drops pass rapidly into the subsequent stages in which thin fibers are extruded, thus reducing the probability for platelet puncture.

When shorter alkanes C_{14} and C_{15} are used, the number of breakage events decreases further because of the even faster platelet transformation into the shapes in which thin fibers are extruded, without passing through the stage of flattened platelets with a thinner central region. No drop breakages via Mechanism 1a are observed with C_{14} and C_{15} oils (see Figure 5I−K).

The observed maximum in the number of bursting events, when varying the alkane chain length, is preserved when other surfactants are used. For example, drops stabilized by $C_{16}SorbEO_{20}$ behave qualitatively similar to those stabilized with $C_{18}EO_{20}$. However, because $C_{16}SorbEO_{20}$ is shorter by two C atoms, the behavior of the $C_{14}/C_{16}SorbEO_{20}$ system is similar to that of $C_{16}/C_{18}EO_{20}$, whereas the behavior of $C_{15}/C_{16}SorbEO_{20}$ is similar to that of $C_{17}/C_{18}EO_{20}$. Drops stabilized by the $C_{18}SorbEO_{20}$ surfactant burst rarely because a very thick frame of rotator phase is formed with C_{16} in this system (and this is the alkane for which one may expect the largest number of bursting events with this surfactant because of their similar chain lengths).

Effect of Surfactant Type for Different Alkanes. In our previous study,[24] we classified the surfactants into four groups, with respect to their effect on drop-shape changes upon cooling. These groups are Groups A−C—surfactants which induce self-

DOI: 10.1021/acs.langmuir.7b02048
Langmuir 2017, 33, 12155−12170

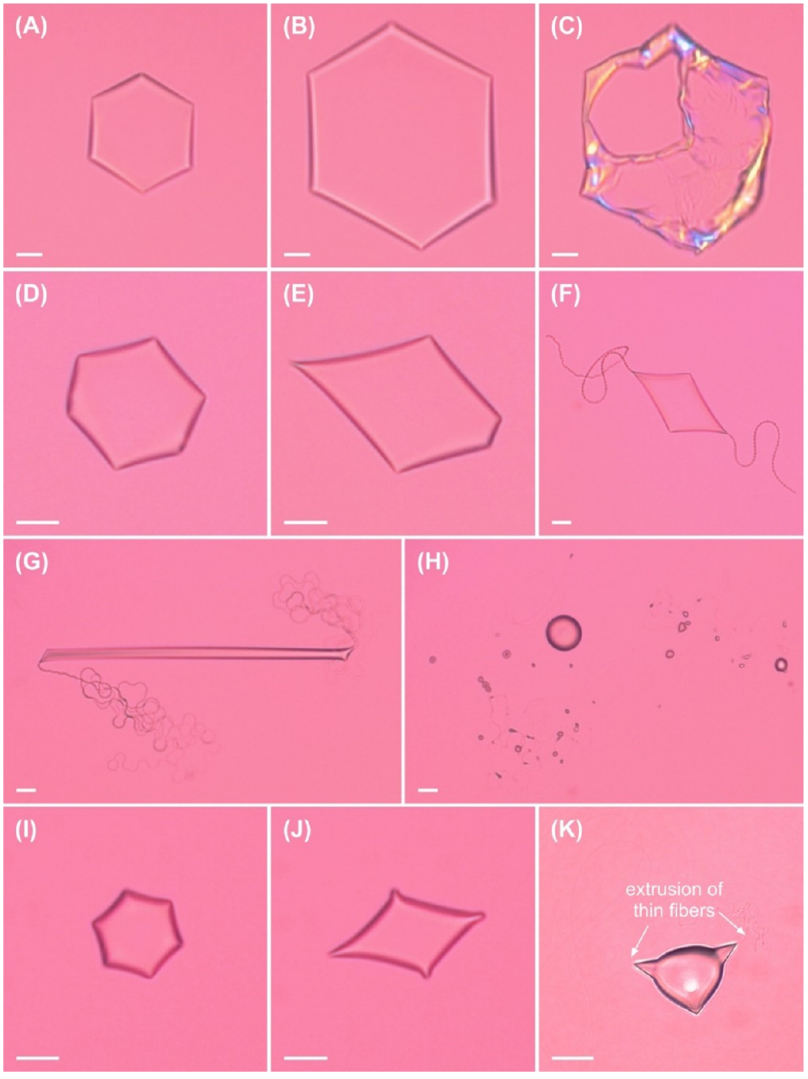

Figure 5. Microscope images showing platelet formation and fiber extrusion for different alkanes. (A–C) C_{19} drops stabilized by $C_{18}EO_{20}$. Upon cooling, these drops deform into thin hexagonal platelets and freeze without passing into the next stages of the evolutionary scheme. (D–H) C_{16} drops stabilized by $C_{18}EO_{20}$. These drops form thin platelets prior to fiber extrusion. The rodlike (G) and capillary instability stages (H) are passed before these drops become ellipsoidal and start extruding thin fibers. (I–K) C_{14} drops stabilized by $C_{18}EO_{20}$. Upon cooling, these drops pass from hexagonal into tetragonal platelets when they are still rather bulky (viz., with convex surface, instead of being thin flat platelets as in A–F). The drops start to extrude thin fibers almost immediately after acute corners are formed, and ellipsoidal drops are formed soon afterward, without passing through the stages of thin flat platelets and rods.

shaping but the deformations start at different temperatures, T_d, as compared to the bulk melting temperature of the emulsified alkane, T_m; for Group A, $T_d > T_m$; for Group B, $T_d \approx T_m$; and for Group C, $T_d < T_m$ and Group D—surfactants that do not induce self-shaping (see Table 2).

Drop-bursting via Mechanism 1 is observed mainly with surfactants from Group A. For drops stabilized by these surfactants, we observed up to more than 10 consecutive breakage events, most typically between 2 and 8. Surfactants from Group B induce usually between one and three breakage events, whereas drop breakage with surfactants from Group C is rarely observed.

Although all surfactants from Group A induce many breakage events, the behavior of the various systems is different. Drop-shape transformations for C_{16} drops, stabilized by surfactants with 10 ethoxy groups ($C_{16}EO_{10}$ and $C_{18}EO_{10}$) start at temperature $T_d \approx T_m + 5$ °C, viz., at $\Delta T = T_d - T_m \approx 5$ °C. The drops in these systems do not have a tendency to form platelets with thin filaments. Instead, irregular-shaped (corrugated) platelets are formed during cooling, resulting in several breakage events in the process of platelet formation. After each of the bursting events, a small number (typically between one and three) of much smaller droplets are formed, and the main fraction of the oil remains in a single drop with diameter close to the initial one (see Movie S1). Thus, the mean volume–surface diameter, d_{32}, does not change significantly, whereas the number diameters d_{N95} and d_{N50} decrease notably. This behavior is observed with C_{16} drops, stabilized by the nonionic surfactants $C_{16}EO_{10}$ and $C_{18}EO_{10}$, and also with C_{18} drops, stabilized by the anionic surfactant $C_{18}SO_4Na$.

The other surfactants from Group A, which tend to form platelets with thin filaments, typically at $\Delta T \approx 1$–4 °C, lead to intensive drop breakage via both Mechanisms 1a and 1b, with the formation of two to six drops of comparable diameter plus several much smaller droplets. In this case, Mechanism 1 is most effective and even comparable in effectiveness to Mechanism 3

DOI: 10.1021/acs.langmuir.7b02048
Langmuir 2017, 33, 12155–12170

Table 2. Surfactant Classification with Respect to the Temperature, T_d, at Which the First Drop Deformation is Observed (See Also Ref 24)

	drop-shape transformations upon cooling	deformation temperature, T_d, compared to bulk melting temperature, T_m	interfacial layers' strength (thickness)	typical number of breakage events in Mechanism 1	surfactants in this group for C_{16} alkane
Group A	yes	$T_d > T_m$	thin flexible layers and rods	1−10	$C_{16}EO_{10}$ $C_{18}EO_{10}$ $C_{18}EO_{20}$
Group B	yes	$T_d \approx T_m$	very strong (thick) layers and rods	1−3	$C_{16}SorbEO_{20}$ $C_{18}SorbEO_{20}$
Group C	yes	$T_d < T_m$	intermediate, soft layers and rods	no	$C_{16}EO_{20}$ $C_{16-18}EO_{25}$ $C_{16}TAB$
Group D	no	no	no	no	$C_{12}EO_{23}$ $C_{12}SorbEO_{20}$ $C_{20-40}EO_{50}$

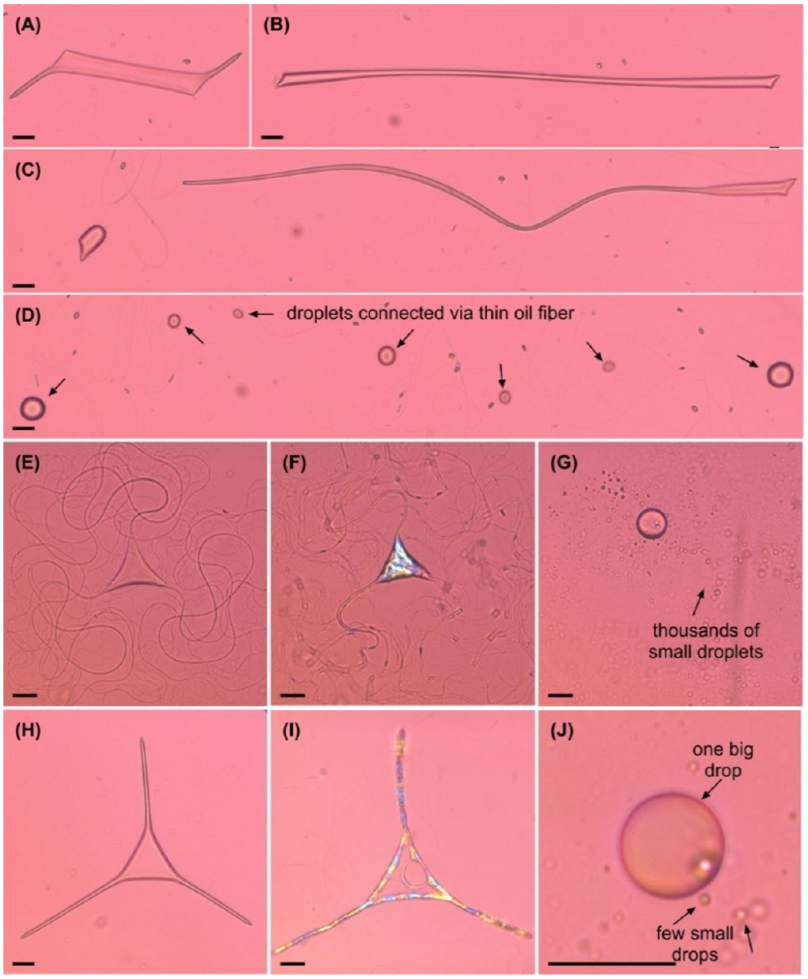

Figure 6. Capillary instability of long fibers (Mechanism 2). (A−D) Upon slow cooling, the drops may undergo shape transition in which the main fraction of the oil reforms into one or several ellipsoidal drops connected to one another with thin fibers. (A) Elongating tetragonal prism. (B−C) Capillary instability. (D) Drops formed after the shape transition has occurred. Experiment with C_{16} drop stabilized by $C_{16}EO_{20}$. (E−J) The fibers, extruded upon cooling, are stabilized by the elasto-plastic properties of the rotator phase. However, upon melting, they break into numerous small droplets via hydrodynamic instability of Rayleigh−Plateau type. (E−G) Breakage observed with fibers of diameter ≈2 μm. C_{15} drop stabilized by $C_{16}EO_{20}$. (H−J) Fibers with diameter ≈4 μm do not disintegrate upon melting. From this triangular platelet with protrusions, one big drop and several small droplets are formed. C_{16} drop stabilized by $C_{16}EO_{20}$. The scale bar is 20 μm.

DOI: 10.1021/acs.langmuir.7b02048
Langmuir 2017, 33, 12155−12170

(melt−crystal fragmentation), as discussed below. In this group, we include the $C_{18}EO_{20}$ surfactant with C_{16} and C_{17} alkanes and $C_{16}SorbEO_{20}$ with C_{14} and C_{15} alkanes.

When the temperature difference ΔT is bigger than 5−6 °C, the formation of thin fibers is quite easy, and the drops start to extrude such fibers even from bulky shapes, without the formation of large flat platelets (see Figure 5I−K). The number of breakage events decreases down to one or two, and they usually lead to the formation of one big drop and one to two small droplets. Hence, the decrease in d_{32} is insignificant in these systems. This behavior is observed with C_{14} and C_{15} drops stabilized by the $C_{18}EO_{20}$ surfactant.

Effect of the Initial Drop Size. Usually, the bigger drops with $d_{ini} \approx 20-30$ μm burst more often than the smaller ones, $d_{ini} \leq 10$ μm. Furthermore, for C_{16} drops stabilized by the $C_{18}EO_{20}$ surfactant, we observe a critical drop diameter, $d_{ini} \approx 12$ μm, below which the drops do not burst anymore. In this system, drops with diameter around 15 μm burst usually only once, whereas 34 μm drops burst between one and six times (most often two or three) when cooled at 1.4 K/min. This trend is explained by considering the kinetics of drop-shape evolution and its dependence on d_{ini}. The small drops always evolve faster to the last stages of the evolutionary scheme, thus passing quicker through the platelet stages.[24] Therefore, the platelets formed from such small drops do not have enough time to thin and burst via Mechanism 1a or 1b. Once the drops are in the last stage of the evolutionary scheme, they cannot burst via Mechanism 1, except in the case of triangular platelets, as already discussed.

In some systems, we observe the opposite dependence on the drop size, which could be also explained with the kinetics of drop-shape transformations. For example, as explained in section Effect of Alkane Chain Length above, it is more difficult for C_{17} drops to evolve into the stage of thin fiber extrusion. Hence, small drops with diameters below 10 μm burst as platelets between 4 and 10 times in this system when cooled at 1.4 K/min, whereas the bigger drops with $d_{ini} \approx 34$ μm evolve much more slowly and burst around 3−4 times only before they freeze.

Effect of the Cooling Rate. The cooling rate influences the number of bursting events in Mechanism 1 in two different ways. The number of bursting events via Mechanism 1a is decreased at a higher cooling rate because the time available for making a thin film in the center of a regular platelet (needed for effectuation of this mechanism) is shorter. On the contrary, when Mechanism 1 occurs via wrinkle formation in the process of platelet formation (1b), the higher cooling rate leads to larger number of bursting events because more dynamic wrinkles are formed. As examples of these trends, C_{17} drops with $d_{ini} \approx 34$ μm, stabilized by $C_{18}EO_{20}$, burst more times when cooled at a low cooling rate (via Mechanism 1a), whereas the C_{16} drops, stabilized by the same surfactant, burst more times when cooled at a higher cooling rate (via Mechanism 1b).

In conclusion, Mechanism 1 is most effective to decrease d_{32} when the breakage occurs via film thinning and breakage in the platelet center (Mechanism 1a) because two to six similar-sized drops are formed in this case. This behavior is observed with oil−surfactant pairs for which $\Delta T \approx 2-3$ °C, and the drops have the tendency to form platelets, protruding thin filaments. All main experimental trends can be explained by considering the effect of the observed drop-shape kinetics on the probability for the realization of Mechanism 1a or Mechanism 1b.

Capillary Instability of the Long Fibers (Mechanism 2). The second mechanism of self-emulsification consists of two stages: Stage 1—formation of thin long fibers upon cooling, which may occur via two different processes, denoted below as Mechanism 2a and Mechanism 2b and Stage 2—disintegration of these fibers in the process of their melting upon heating.

Stage 1 in Mechanism 2. Mechanism 2a. Upon cooling, in the final stages of the evolutionary scheme, we often observe a process in which a platelet or rod spontaneously reshapes into one or several ellipsoidal drops with several sharp conical tips, from which thin fibers are extruded (see Figures 1A and 2). Usually, after this event, the whole oil entity reforms into a single ellipsoidal drop (see Figure 5D−H). However, in some systems, two or three drops of comparable size have been typically observed to form (see Figure 6A−D). These drops are interconnected with very thin fibers of diameter <1 μm. Such multiple drops formation is observed mainly with systems forming initially intermediate and thick rotator phases, that is, with surfactants from Groups B and C, according to the classification in Table 2. If these samples are heated slowly, prior to the final drop-freezing, these apparently separated drops coalesce back and re-form the single initial oil drop, from which they have been obtained (see Movie S2). The latter observation is a direct proof that the ellipsoidal drops formed by this process from one initial drop (e.g., those seen in Figure 6D) are still interconnected by very thin oily fibers before their complete freezing.

In ref 24, we explained this phenomenon with a possible phase transition of type $R_{CI} \rightarrow R_{CV}$, where R denotes the "rotator phase" and the indexes CI and CV denote phases with different molecular arrangements of the alkane molecules (see refs and 24 and 27−33 for detailed explanations of the various rotator phases and their transitions). The observed changes in the drop shape, from platelet/rod into ellipsoidal drops and connecting thin fibers, indicate that the phase transition $R_{CI} \rightarrow R_{CV}$ leads to the formation of a thinner and mechanically weaker rotator phase on the drop surface. This weaker plastic phase (R_{CV}) is unable to counteract the finite oil−water interfacial tension (as the thicker phase R_{CI} did initially) and the rods/platelets are forced by the capillary pressure to reshape into ellipsoidal drops—the thin connecting fibers are formed as a "byproduct" of this shape transformation. As explained in ref 22, these thin fibers are stabilized by the plastic properties of the rotator phase R_{CV}, which precludes the spontaneous fiber fragmentation via the Rayleigh−Plateau type of hydrodynamic instability.

Mechanism 2b. Thin fibers with a diameter between ca. 0.5 and 5 μm spontaneously occur and gradually protrude from the platelet corners in many of the evolutionary stages, observed in the drop-shape evolution upon cooling (see Figures 1A and 6E,H). These fibers are stable upon cooling and freezing because of the elasto-plastic rigidity of the rotator phase.[22] However, they break upon melting as described below.

Stage 2 in Mechanism 2. Upon melting, the fibers formed in Stage 1 split into numerous small droplets with a diameter around 2 times bigger than the fiber diameter. These observations evidence that the cylindrical fibers disintegrate in the moment of oil melting as a result of hydrodynamic instability of Rayleigh−Plateau type (Figure S2).[22] If the fibers connect the ellipsoidal drops before freezing, as described in Mechanism 2a above, these ellipsoidal drops become truly separated after melting, reducing the initial drop volume by 2−3 times and the respective drop diameter by 20−30%.

This stage is operative only for fibers with a diameter around or below 2.5 μm. From such fibers, hundreds of small drops are formed upon melting. For example, if a fiber is 1000 μm long and has a radius, $R_f \approx 0.5$ μm, the radius of the formed drops is $R_d \approx$

DOI: 10.1021/acs.langmuir.7b02048
Langmuir 2017, 33, 12155−12170

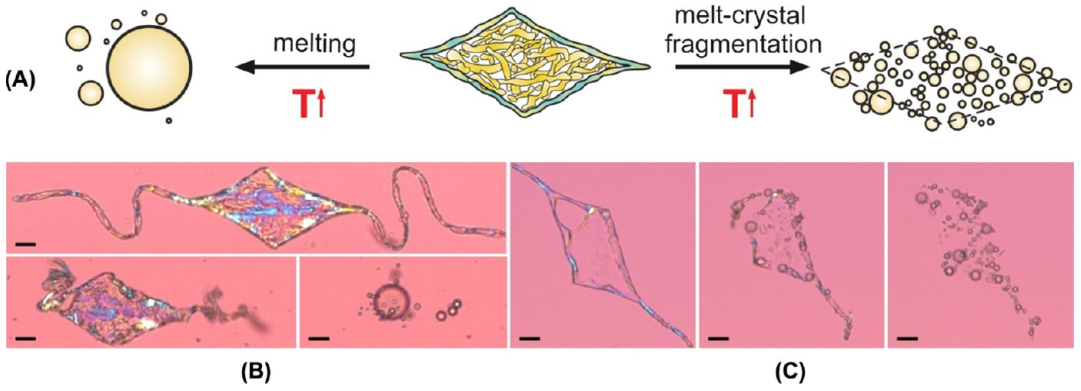

Figure 7. Melt−crystal fragmentation process (Mechanism 3). (A) Upon heating, platelets may melt into one big drop and several smaller droplets (B) or directly fragment into hundreds of small drops (C). (B) Typical melting process into one big and several small droplets, as observed with the C_{16} drop stabilized by $C_{16}EO_{20}$. (C) Process of melt−crystal fragmentation leading to the formation of numerous small droplets, as observed with the C_{17} drop stabilized by $C_{18}EO_{20}$. The scale bar is 20 μm.

$2R_f$ and the number of newly formed droplets is estimated to be >200, just from this single fiber (most of the drops extrude usually two or three fibers which may be much longer than the length used for this estimate). Thus, hundreds or thousands of small droplets are formed from one oil drop after just one freeze−thaw cycle (see Figure 6E−G). By contrast, the thicker fibers melt slowly and are able to re-form back into a single drop, as shown in Figure 6H−J, with C_{16} drops stabilized by $C_{16}EO_{20}$.

This mechanism is extremely operative for reducing d_{N95} and d_{N50}, making them around and below 1 μm, after only one freeze−thaw cycle for the systems in which Mechanism 2b is operative (see Table 1). It is also effective for reducing d_{32} when Mechanism 2a is operative (see Table 1 and Discussion section below).

Effect of Alkane Chain Length. Mechanism 2 is most effective when the drops evolve up to the final stages of the evolutionary scheme before freezing. Thus, alkane molecules which are shorter than the surfactant tail length are most prone to be involved in Mechanism 2. The systems for which Mechanism 2b is most pronounced include C_{14}, C_{15}, C_{16}, and C_{17} emulsions stabilized by $C_{18}EO_{20}$ or $C_{18}SO_4Na$; C_{14} and C_{15} emulsions stabilized by $C_{16}SorbEO_{20}$ or $C_{18}SorbEO_{20}$; C_{14}, C_{15}, and C_{16} emulsions stabilized by $C_{16}EO_{20}$; and C_{14} emulsions stabilized by $C_{16}TAB$. With all these systems, intensive fiber formation is observed if slow cooling rate and appropriate initial drop size are used.

The effectiveness of Mechanism 2a depends also on the thickness of the rotator phase formed on the drop surface. For example, the rotator phase is very fragile in the C_{14} + $C_{18}EO_{20}$ emulsion, and the drops start extruding fibers even from bulky shapes without passing through the capillary instability stage, as it would be the case with C_{16}. Thus, Mechanism 2b is operative in the C_{14} + $C_{18}EO_{20}$ emulsion, whereas Mechanism 2a is not observed in this system. By contrast, if C_{14} is used with sorbitan surfactants, the drops evolve up to the final stages of the evolutionary scheme, passing through the capillary instability stage, and both Mechanisms 2a and 2b are observed.

Effect of Surfactant Type. For C_{16} alkane, the drops with $d_{ini} \approx 34$ μm stabilized by sorbitan surfactants (from Group B), evolve only up to the flat platelet stage, and Mechanism 2 is not operative. By contrast, C_{16} emulsions stabilized by surfactants from Group A and C can evolve up to the final stages of the evolutionary scheme, and Mechanism 2 is active upon heating. As already explained, when shorter alkanes are used (C_{14} or C_{15}), the surfactants from Group B (as classified for C_{16}) can form thinner rotator phases, and respectively, the drops in these emulsions may evolve into the final stages of the evolutionary scheme. Correspondingly, drop disintegration via Mechanism 2 is observed upon subsequent heating with such short-chain alkanes, even with sorbitan surfactants (see Table 1).

Effect of the Initial Drop Size and Cooling Rate. The drops with a smaller initial diameter and cooled at lower rates evolve up to the further stages of the evolutionary scheme. Therefore, these drops are more likely to extrude fibers and undergo capillary instability upon cooling. Upon heating after freezing, the fibers with a diameter less than 2.5 μm disintegrate in such systems, forming numerous small droplets.

In conclusion, Mechanism 2 is most operative for emulsions in which the chain length of the oil is slightly shorter than the chain length of the surfactant tail because the drops in these systems usually evolve to the final stages of the evolutionary scheme. Mechanism 2a is operative for the reduction of volume−surface diameter, d_{32}, whereas Mechanism 2b is extremely effective in reducing the number diameters, d_{N95} and d_{N50}, when fibers with a diameter <2 μm are formed upon cooling.

Melt−Crystal Fragmentation (Mechanism 3). The third mechanism for decreasing the emulsion drop size consists of bursting (fragmentation) of frozen platelets at the moment of their melting (Figure 7A). Our observations showed that the crystal domains in the platelet melt within a period of several seconds. In the systems stabilized with appropriate surfactants, the liquid (just melted) alkane domains dewet (separate from) the still frozen crystalline alkane domains so that a single platelet splits into hundreds of separate droplets.[22]

Effect of the Initial Drop Size and Cooling Rate on Melt−Crystal Fragmentation. Mechanism 3 is effective only for frozen platelets formed upon cooling. The bulky shapes which may form if the drops freeze in the initial stages of drop evolution as well as the frozen ellipsoidal drops formed after the shape transitions in the last stages of drop evolution do not fragment by Mechanism 3 upon heating. Therefore, the effectiveness of this mechanism depends primarily on the particle shapes formed upon drop-freezing.

For a given alkane−surfactant pair, the particle shapes obtained upon freezing depend on the initial drop size and cooling rate.[24] In general, drops with diameters less than 10 μm easily evolve up to the final stages of the evolutionary scheme, even at a cooling rate of 1.5 K/min. The obtained ellipsoidal

DOI: 10.1021/acs.langmuir.7b02048
Langmuir 2017, 33, 12155−12170

drops do not disintegrate upon heating, as explained above. Therefore, higher cooling rates are more appropriate in such emulsions for realization of Mechanism 3. As an example, the mean drop diameter d_{V50} is ≈ 4.6 μm after one F/T cycle for C_{16} emulsion drops with d_{ini} ≈ 11 μm stabilized by $C_{18}EO_{20}$, when cooled at 1.5 K/min, whereas this size is d_{V50} ≈ 2.8 μm when the same emulsion is cooled at 20 K/min.

The bigger drops with d_{ini} > 20 μm need cooling rates lower than 1 K/min to transform into platelets. Therefore, low cooling rates are more appropriate for the large droplets.

Effect of Surfactant–Alkane Combination. Preparation of frozen platelets is a required step for the occurrence of Mechanism 3; however, it is insufficient. As seen from Figure 7B,C, platelets with the same shape may or may not fragment upon melting, depending on the specific alkane–surfactant pair. The systems in which Mechanism 3 is very pronounced include C_{16}, C_{17}, and C_{18} emulsions stabilized by $C_{18}EO_{20}$; C_{14} and C_{15} emulsions stabilized by $C_{16}SorbEO_{20}$; and C_{16} emulsion stabilized by $C_{18}EO_{10}$. All these systems classify as emulsions, corresponding to surfactants from Group A (see Table 1). Thin platelets are formed in these emulsions upon cooling.

Effect of Heating Rate. As the melt–crystal fragmentation is observed during sample heating, one may expect this process to be affected by the heating rate. To check this possibility, we performed experiments at different heating rates, varied within 2 orders of magnitude, between 0.1 and 10 K/min. However, we did not observe any significant difference in sample behavior upon melting within this range of heating rates (for fixed all other conditions). The obtained drops after one or several freeze–thaw cycles had similar size distributions, and the latter were influenced by the cooling rates only.

Analyzing the various physicochemical properties for the systems involved in Mechanism 3, we observed one common feature. For all systems exhibiting Mechanism 3, the interfacial tension of the surfactant solution–oil, $\sigma(T)$, decreases when the temperature is lowered toward the bulk melting temperature of oil, T_m (see Figure 8). This trend is explained with the formation of a compact (dense) adsorption layer on the platelet surface before it freezes (see Figure 4e in ref 26). As a result, the interfacial tension of the frozen alkane domains covered with such dense surfactant layers is lower, and they are more easily dewetted by the released melted alkane droplets upon platelet melting. As explained in ref 22, this dewetting process is crucial for the observed platelet bursting into small droplets via Mechanism 3. Most appropriate for realization of this mechanism are the surfactants with the tail length comparable to or slightly longer than the length of the alkane molecules.[22] In these systems, the drop deformation starts above the melting temperature of the bulk oil, T_m, viz., these are the surfactants from Group A, according to the classification in ref 24.

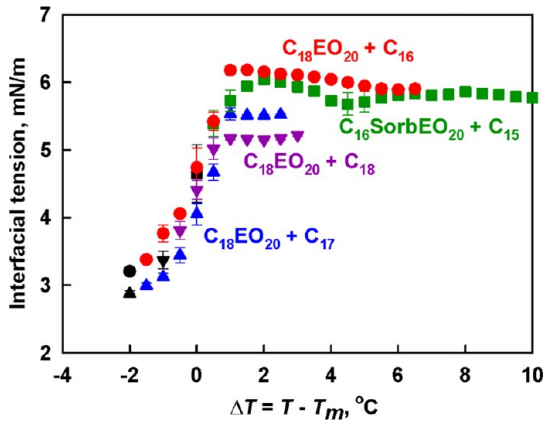

Figure 8. Dependence of the interfacial tension on the temperature difference, $\Delta T = T - T_m$, between the temperature of the sample and the bulk melting temperature of the alkane for the systems exhibiting Mechanism 3 (see Table S1). For all systems, in which Mechanism 3 is pronounced, the interfacial tension decreases when T approaches T_m from above.

However, our experiments showed that this decrease in the interfacial tension with the decrease in the temperature is not a sufficient condition for self-emulsification via Mechanism 3. For example, a decrease of the interfacial tension is observed with C_{16} drops stabilized by the C_{18}TAB surfactant.[26,46] Nevertheless, no intensive crystal–melt fragmentation is observed upon melting of the platelets formed in the respective emulsions (see Figure S3).

With alkane–surfactant pairs, for which no decrease of interfacial tension is observed, a process of melt–crystal fragmentation has not been observed either.

In conclusion, Mechanism 3 is most effective for thin frozen platelets formed upon emulsion cooling. To prepare such platelets, different cooling rates need to be applied, depending on the initial drop size; the bigger the drops, the lower cooling rate is needed. Intensive melt–crystal fragmentation may be expected only for the systems in which a decrease of the interfacial tension is observed around T_m upon cooling.

Discussion—Comparison of the Relative Effectiveness of Different Mechanisms. In this section, we compare for the first time the effectiveness of the different mechanisms of self-emulsification, with respect to the observed drop-size decrease. For this purpose, we use the decrease in the mean volume–surface diameter of the drops, d_{32}, and the following relation

$$\text{Effectiveness} = 1 - \frac{d_{32}}{d_{32,ini}}$$

where $d_{32,ini}$ is the mean drop diameter in the initial emulsion and d_{32} is the mean drop diameter in the emulsion obtained after the cooling–heating cycle(s). If d_{32} is not changed significantly after the cooling–heating cycle, the effectiveness is close to zero, whereas a very significant decrease in d_{32} corresponds to effectiveness approaching 100%.

Effectiveness of Mechanism 1. To determine the effectiveness of Mechanism 1 only, we performed the following type of experiment: we measured the initial drop size distribution, cooled the sample down to a temperature which was just above the freezing temperature of the drops, and then heated the drops back to their liquid state. In this experiment, the drops are not solidified, and thus the drop size decrease is exclusively due to Mechanism 1.

For oil drops with $d_{32,ini}$ ≈ 34 μm stabilized by $C_{18}EO_{20}$, the drop size decreased to d_{32} ≈ 18 μm for C_{17} and to ≈23 μm for C_{16} after such an experiment with a cooling rate of 0.2 K/min. Therefore, the effectiveness of Mechanism 1 was ≈30% (for C_{16}) and ≈50% (for C_{17}) at this cooling rate. The latter result for C_{17} is shown by the empty square in Figure 9A. At a higher cooling rate of 1.4 K/min, the effectiveness was lower; see the empty triangle in Figure 9A.

When a whole F/T cycle was applied to the same emulsions, the drop size became d_{32} ≈ 4.4 μm for C_{17} and d_{32} ≈ 15 μm for C_{16} for 0.2 K/min cooling rate. In this type of experiment, when the drops freeze upon cooling, all three mechanisms are operative

DOI: 10.1021/acs.langmuir.7b02048
Langmuir 2017, 33, 12155–12170

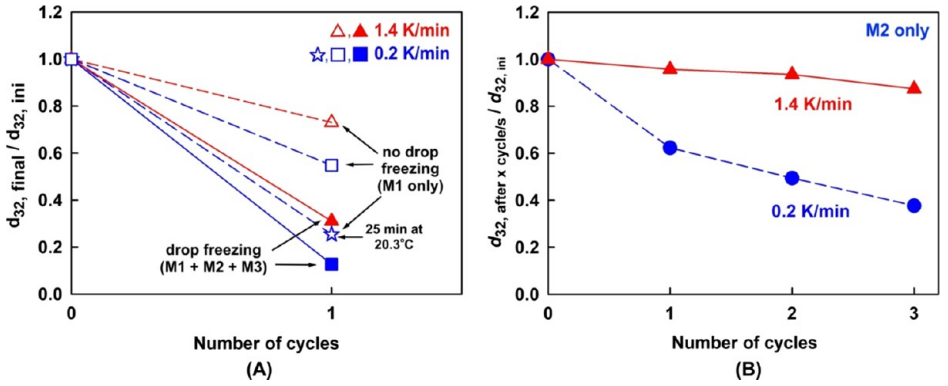

Figure 9. (A) Relative effectiveness of Mechanism 1. Comparison between the effectiveness of Mechanism 1 and the combined effectiveness of all three mechanisms. The graphs present the ratio between the final d_{32} diameter and the initial $d_{32,ini}$ diameter as a function of the number of cycles. Cycle "0" denotes the original sample and cycle "1" corresponds to one cycle, which might be performed without freezing of the drops (empty symbols) or with freezing of the drops (solid symbols). The star symbol presents the results from an experiment in which the sample is cooled to T = 20.3 °C, and this temperature is maintained for 25 min without drop-freezing, before the sample is heated back to room temperature. All experiments in (A) are performed with C_{17} drops, $d_{32,ini} \approx 34$ μm, surfactant $C_{18}EO_{20}$. Drops are cooled at two different rates, 0.2 K/min (blue symbols) and 1.4 K/min (red symbols). (B) Effectiveness of Mechanism 2. Drop-size decrease via Mechanism 2 in the system $C_{16}/C_{16}EO_{20}$, $d_{32,ini} \approx 34$ μm. Red symbols present data for cooling rates of 1.4 K/min and the blue symbols present those of 0.2 K/min; the heating rate is always 1.6 K/min.

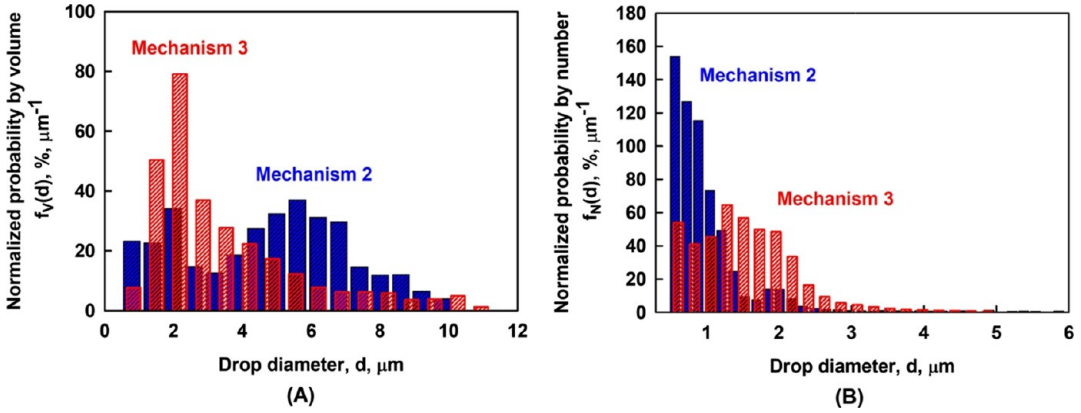

Figure 10. Relative effectiveness of Mechanism 3. Comparison between the drop size distributions (A) by volume and (B) by number, obtained after one F/T cycle at two cooling rates—0.2 K/min (blue bars, Mechanism 2 prevailing) and 20 K/min (red bars, Mechanism 3 dominating). In both cases, the heating rate is 1.6 K/min. These experiments are performed with C_{16} drops with $d_{ini} \approx 11$ μm, stabilized by $C_{18}EO_{20}$.

for the drop-size decrease. Thus, the combined action of all three mechanisms leads to a drop-size decrease by 55% (for C_{16}) and by 85% (for C_{17}, see the solid square in Figure 9A). At a higher cooling rate of 1.4 K/min, the combined effectiveness of the three mechanisms is again lower (solid triangle in Figure 9A). Summarizing, Mechanism 1 contributes to ≈60% of the total effectiveness of the whole F/T cycle when the decrease in d_{32} is compared.

As already discussed, to observe bursting via Mechanism 1, the drops need time to deform until they thin locally and break. To check whether we can improve the effectiveness of Mechanism 1 by providing more time for drop deformation, we performed another type of experiment. We cooled the sample to a temperature slightly above the platelet freezing temperature and maintained this temperature for 25 min before heating up the emulsion. As seen from the empty star symbol in Figure 9A, Mechanism 1 was much more effective in this experiment and led to a drop-size decrease by around 75%. Therefore, we could improve significantly the effectiveness of Mechanism 1 using a properly optimized cooling regime.

Effectiveness of Mechanism 2. The separate effectiveness of Mechanism 2 can be determined from the data for the drop-size decrease of C_{16} drops stabilized by $C_{16}EO_{20}$, for which only this mechanism is operative (see Table 1). Figure 9B presents the data for drops with $d_{32,ini} \approx 34$ μm, after three consecutive F/T cycles. At a cooling rate of 1.4 K/min, the drop size does not change even after three cycles. At this cooling rate, the drops evolve up to the platelet stages, but the platelets melt back into a single drop upon heating. At a cooling rate of 0.2 K/min, however, the drop size decreases slowly. At this cooling rate, the drops pass through the whole evolutionary scheme, including the stage of capillary instability. As discussed in section Stage 1, Mechanism 2a above, the drops stabilized by the surfactant from Group B or C (Table 2) usually separates its volume into two or three ellipsoidal drops after the process of capillary instability (see Figure 6A–D). Thus, the drop-size decrease in the $C_{16}/C_{16}EO_{20}$ emulsion is only due to Mechanism 2. Note that the observed decrease in d_{32} is mainly due to Mechanism 2a, whereas the decrease in d_{N95} is mainly due to Mechanism 2b. The overall effectiveness of Mechanism 2 after one F/T cycle is ≈40% decrease in d_{32}.

Effectiveness of Mechanism 3. This mechanism is most operative when frozen platelets are formed. To isolate this mechanism from the others, we performed "shock" cooling of a C_{16} emulsion with $d_{ini} \approx 11$ μm, stabilized by $C_{18}EO_{20}$ at a cooling rate of ≈20 K/min. At such a high cooling rate, the drops

DOI: 10.1021/acs.langmuir.7b02048
Langmuir 2017, 33, 12155−12170

(which normally would evolve through the whole evolutionary scheme) transform up to the platelet stage and freeze. When this emulsion was heated and the platelets melted, melt−crystal fragmentation via Mechanism 3 was observed, whereas Mechanisms 1 and 2 were not operative (see Movie S3).

The decrease of d_{32} in the above experiment was ≈75%. The respective histogram of the drop size distribution by volume, after one F/T cycle, is presented with red bars in Figure 10 (the histograms for the initial emulsions are presented in Figure S4). As seen from Figure 10A, the drop size distribution by volume is log-normal, with a peak around 2 μm. The respective d_{V50} diameter is ≈2.8 μm. Most of the drops have diameters between 0.5 and 2.5 μm, as seen from the histogram by number (Figure 10B, red bars). Very similar results were obtained with C_{17} emulsions with $d_{ini} \approx 34$ μm, stabilized by $C_{18}EO_{20}$.

For comparison, with blue bars in the same figure, we present the drop size distributions obtained when the experiment with the same initial C_{16} emulsion is performed at a low cooling rate of 0.2 K/min. In this case, 11 μm C_{16} drops stabilized by $C_{18}EO_{20}$ transform through the whole evolutionary scheme, eventually forming ellipsoidal drops, which extrude thin fibers before freezing. These drops do not burst via Mechanism 1, and thus the drop-size decrease is mainly due to Mechanism 2. The mean volume−surface diameter after one F/T cycle at a cooling rate of 0.2 K/min is very similar to that obtained after "shock" cooling, $d_{32} \approx 2.7$ μm at 0.2 K/min and $d_{32} \approx 2.6$ μm at 20 K/min. However, as seen from the histograms, these two emulsions have very different drop size distributions. After slow cooling of 0.2 K/min, the emulsion obtained via Mechanism 2 has bimodal distribution by volume, with peaks around 2 and 5.5 μm, Figure 10A (blue bars). The drop size distribution by number is log-normal, and most of the drops have diameters around 1 μm ($d_{N84} \approx 1.4$ μm and $d_{N95} \approx 2.2$ μm). The reason is that the thin fibers, extruded upon cooling, disintegrate upon heating and form thousands of small droplets, whereas the main fraction of the oil remains in the large ellipsoidal drops, which do not undergo melt−crystal fragmentation (it requires melting platelets) and remain as large melted drops after the cycle.

In conclusion, Mechanism 3 may reduce d_{32} by around 75% after just one F/T cycle. For small drops, which can evolve up to the last stage of the evolutionary scheme, this effectiveness is comparable with the effectiveness of Mechanism 2. However, when the drops reduce their size by Mechanism 2, the obtained emulsions are typically bimodal, whereas Mechanism 3 leads to monomodal log-normal distribution by volume, as usually observed with the conventional emulsification methods.

CONCLUSIONS

We present a systematic study with a wide range of alkane−surfactant pairs of the mechanisms leading to drop-bursting and self-emulsification in cyclically cooled−heated emulsions. The obtained results reveal that this process can be applied to various systems, and three main mechanisms are responsible for the observed drop-bursting process. In the current study, we show the following:

Most effective for the drop-size decrease is Mechanism 3 (melt−crystal fragmentation), for which d_{32} may decrease by more than 75% after a single F/T cycle if appropriate conditions are used. For large initial drops (ca. 20−40 μm), this may require slow cooling, whereas for smaller initial drops (ca. 5−15 μm), faster cooling may be required to freeze the deformed drops at the stage of flat platelets.

The effectiveness of Mechanism 1 (puncture of the fluid platelets upon cooling), characterized by the observed decrease of d_{32} after one cooling−heating cycle, is around 40%, though this can be increased up to 75% if an appropriate cooling protocol is applied. For example, we have observed this when the drops were cooled to a temperature, which is just above their freezing temperature and the emulsion is stored at this temperature for a longer period of time (e.g., 15−30 min), which ensures more time for drop deformation and puncturing.

The effectiveness of Mechanism 2 (hydrodynamic instability of melting fibers) depends strongly on the initial drop size and the cooling rate because the bigger drops need much longer time to evolve to the final stages of the evolutionary process and to extrude the same fraction of oil as compared to the smaller drops (the extruded fibers are with a similar diameter for given alkane−surfactant pair, no matter the drop size). For big drops, the effectiveness of Mechanism 2 is around 40%, whereas for small drops, it can reach the effectiveness of Mechanism 3 (up to 75%). However, drops formed in Mechanism 2 usually have bimodal distribution, whereas the emulsions are with much smaller polydispersity when Mechanism 3 is predominant.

These results show that the self-emulsification procedure via F/T cycles of the dispersed drops could be very effective under appropriate conditions. These conditions could be optimized to improve the effectiveness and to control (to some extent) the drop size distribution. The main advantages of this procedure are (1) the low temperature of emulsion handling, without unnecessary heating that could deteriorate the temperature-sensitive ingredients; (2) the possibility to form micrometer and submicrometer droplets after one to several F/T cycles; and (3) the scalability to industrial capacities at relatively high energy efficiency.[22]

Most appropriate for realization of this self-emulsification procedure are the surfactants with tail length comparable to or slightly longer than the length of the alkane molecules, for which the drop deformation starts above the melting temperature of the bulk oil, T_m, viz., those falling in Group A, according to the classification from ref 24. The selection of appropriate cooling protocol is very important to obtain significant reduction of the drop diameter, d_{32}, by activating the most appropriate mechanism(s) for the respective alkane−surfactant pair. With the best surfactants, we observed the formation of droplets with a mean radius of ca. 300 nm (Figure 6c in ref 22). This radius is in agreement with our estimate[23−26] that the thickness of the plastic phase in the systems studied is of the order of 10^2 nm.

In our previous studies, this self-emulsification process was observed also with fatty alcohols and triglycerides as dispersed oily drops[22] as well as with mixtures of alkanes with different chain lengths.[25] In the latter case, a separate, fourth mechanism of self-emulsification was observed.[25] It is due to drop disintegration upon freezing for the alkane mixtures with large gaps in the consecutive chain lengths, $\Delta n > 4$. This mechanism includes freezing of the different components at different temperatures, thus forming phase-separated crystalline domains of the longer and shorter alkane components.

ASSOCIATED CONTENT

Supporting Information

The Supporting Information is available free of charge on the ACS Publications website at DOI: 10.1021/acs.langmuir.7b02048.

DOI: 10.1021/acs.langmuir.7b02048
Langmuir 2017, 33, 12155−12170

Tables of properties of alkanes and surfactants studied, diagram of the experimental setup, and figures illustrating specific instances of drop size distributions and drop-bursting mechanisms (PDF)

Drop-shape evolution upon cooling of C_{16} drops with an initial diameter, $d_{ini} \approx 33$ μm, stabilized by the $C_{16}EO_{10}$ surfactant (AVI)

Drop-shape evolution upon cooling of C_{16} drops with an initial diameter, $d_{ini} \approx 10$ μm, stabilized by the $C_{16}EO_{20}$ surfactant (AVI)

Self-emulsification via Mechanism 3 (AVI)

AUTHOR INFORMATION

Corresponding Author

*E-mail: s.smoukov@qmul.ac.uk. Phone: +44 20 7882 5305. Fax: (01223) 762088.

ORCID

Stoyan K. Smoukov: 0000-0003-1738-818X

Notes

The authors declare no competing financial interest.

ACKNOWLEDGMENTS

The authors gratefully acknowledge the financial support to S.K.S., EMATTER (# 280078) and Proof-of-Concept ShipShape (# 766656) by the European Research Council (ERC) and by the Scientific Research Fund of Sofia University (project no. 80-10-225). The study falls under the umbrellas of the European network COST MP 1305 and the Horizon 2020 project "Materials Networking" (ID: 692146-H2020-eu.4.b). The authors are grateful to Dr. Ivan Lesov (Sofia University) for the useful discussions.

REFERENCES

(1) Walstra, P.; Geurts, T.; Noomen, A.; Jellema, A.; van Boekel, A. A. J. S. *Dairy Technology*; Marcel Dekker: New York, 1999.

(2) Walstra, P. Formation of emulsions. *Encyclopedia of Emulsion Technology*; Marcel Dekker: New York, 1983; Chapter 2.

(3) Schubert, H.; Engel, R. Product and formulation engineering of emulsions. *Chem. Eng. Res. Des.* **2004**, *82*, 1137−1143.

(4) Coulaloglou, C. A.; Tavlarides, L. L. Description of interaction processes in agitated liquid-liquid dispersions. *Chem. Eng. Sci.* **1977**, *32*, 1289−1297.

(5) Calabrese, R. V.; Chang, T. P. K.; Dang, P. T. Drop breakup in turbulent stirred-tank contactors. Part I: Effect of dispersed-phase viscosity. *AIChE J.* **1986**, *32*, 657−666.

(6) Davies, J. T. Drop sizes of emulsions related to turbulent energy dissipation rates. *Chem. Eng. Sci.* **1985**, *40*, 839−842.

(7) Sprow, F. B. Distribution of drop sizes produced in turbulent liquid−liquid dispersion. *Chem. Eng. Sci.* **1967**, *22*, 435−442.

(8) Vladisavljević, G. T.; Williams, R. A. Recent developments in manufacturing emulsions and particulate products using membranes. *Adv. Colloid Interface Sci.* **2005**, *113*, 1−20.

(9) Christov, N. C.; Ganchev, D. N.; Vassileva, N. D.; Denkov, N. D.; Danov, K. D.; Kralchevsky, P. A. Capillary mechanisms in membrane emulsification: oil-in-water emulsions stabilized by Tween 20 and milk proteins. *Colloids Surf., A* **2002**, *209*, 83−104.

(10) Bibette, J.; Leal Calderon, F.; Poulin, P. Emulsions: basic principles. *Rep. Prog. Phys.* **1999**, *62*, 969−1033.

(11) Mason, T. G.; Wilking, J. N.; Meleson, K.; Chang, C. B.; Graves, S. M. Nanoemulsions: formation, structure, and physical properties. *J. Phys.: Condens. Matter* **2006**, *18*, R635−R666.

(12) Solans, C.; Solé, I. Nano-emulsions: formation by low-energy methods. *Curr. Opin. Colloid Interface Sci.* **2012**, *17*, 246−254.

(13) Perazzo, A.; Preziosi, V.; Guido, S. Phase inversion emulsification: Current understanding and applications. *Adv. Colloid Interface Sci.* **2015**, *222*, 581−599.

(14) Shahidzadeh, N.; Bonn, D.; Meunier, J.; Nabavi, M.; Airiau, M.; Morvan, M. Dynamics of spontaneous emulsification for fabrication of oil in water emulsions. *Langmuir* **2000**, *16*, 9703−9708.

(15) Shahidzadeh, N.; Bonn, D.; Aguerre-Chariol, O.; Meunier, J. Spontaneous emulsification: relation to microemulsion phase behaviour. *Colloids Surf., A* **1999**, *147*, 375−380.

(16) Shahidzadeh, N.; Bonn, D.; Meunier, J. A new mechanism of spontaneous emulsification: Relation to surfactant properties. *Europhys. Lett.* **1997**, *40*, 459−464.

(17) Pouton, C. W. Formulation of self-emulsifying drug delivery systems. *Adv. Drug Delivery Rev.* **1997**, *25*, 47−58.

(18) Gursoy, R. N.; Benita, S. Self-emulsifying drug delivery systems (SEDDS) for improved oral delivery of lipophilic drugs. *Biomed. Pharmacother.* **2004**, *58*, 173−182.

(19) Sitnikova, N. L.; Sprik, R.; Wegdam, G.; Eiser, E. Spontaneously formed *trans*-anethol/water/alcohol emulsions: mechanism of formation and stability. *Langmuir* **2005**, *21*, 7083−7089.

(20) Vitale, S. A.; Katz, J. L. Liquid droplet dispersions formed by homogeneous liquid−liquid nucleation: "The Ouzo effect". *Langmuir* **2003**, *19*, 4105−4110.

(21) Ganachaud, F.; Katz, J. L. Nanoparticles and nanocapsules created using the Ouzo effect: Spontaneous emulsification as an alternative to ultrasonic and high-shear devices. *ChemPhysChem* **2005**, *6*, 209−216.

(22) Tcholakova, S.; Valkova, Z.; Cholakova, D.; Vinarov, Z.; Lesov, I.; Denkov, N.; Smoukov, S. K. Efficient Self-Emulsification via Cooling-Heating Cycles. *Nat. Commun.* **2017**, *8*, 15012.

(23) Denkov, N.; Tcholakova, S.; Lesov, I.; Cholakova, D.; Smoukov, S. K. Self-shaping of oil droplets via the formation of intermediate rotator phases upon cooling. *Nature* **2015**, *528*, 392−395.

(24) Cholakova, D.; Denkov, N.; Tcholakova, S.; Lesov, I.; Smoukov, S. K. Control of drop shape transformations in cooled emulsions. *Adv. Colloid Interface Sci.* **2016**, *235*, 90−107.

(25) Cholakova, D.; Valkova, Z.; Tcholakova, S.; Denkov, N.; Smoukov, S. K. "Self-Shaping" of multicomponent drops. *Langmuir* **2017**, *33*, 5696−5706.

(26) Denkov, N.; Cholakova, D.; Tcholakova, S.; Smoukov, S. K. On the mechanism of drop self-shaping in cooled emulsions. *Langmuir* **2016**, *32*, 7985−7991.

(27) Small, D. M. *The Physical Chemistry of Lipids. From Alkanes To Phospholipids*; Plenum: New York, 1986.

(28) Sirota, E. B.; King, H. E.; Singer, D. M.; Shao, H. H. Rotator phases of the normal alkanes: An x-ray scattering study. *J. Chem. Phys.* **1993**, *98*, 5809−5824.

(29) Sirota, E. B.; Singer, D. M. Phase transitions among the rotator phases of the normal alkanes. *J. Chem. Phys.* **1994**, *101*, 10873−10882.

(30) Sirota, E. B.; Herhold, A. B. Transient phase-induced nucleation. *Science* **1999**, *283*, 529−532.

(31) Ueno, S.; Hamada, Y.; Sato, K. Controlling polymorphic crystallization of n-alkane crystals in emulsion droplets through interfacial heterogeneous nucleation. *Cryst. Growth Des.* **2003**, *3*, 935−939.

(32) Shinohara, Y.; Takamizawa, T.; Ueno, S.; Sato, K.; Kobayashi, I.; Nakajima, M.; Amemiya, Y. Microbeam X-Ray diffraction analysis of interfacial heterogeneous nucleation of *n*-hexadecane inside oil-in-water emulsion droplets. *Cryst. Growth Des.* **2008**, *8*, 3123−3126.

(33) Shinohara, Y.; Kawasaki, N.; Ueno, S.; Kobayashi, I.; Nakajima, M.; Amemiya, Y. Observation of the transient rotator phase of *n*-hexadecane in emulsified droplets with time-resolved two-dimensional small- and wide-angle X-Ray scattering. *Phys. Rev. Lett.* **2005**, *94*, 097801.

(34) Haas, P. A.; Goldstein, R. E.; Smoukov, S. K.; Cholakova, D.; Denkov, N. Theory of shape-shifting droplets. *Phys. Rev. Lett.* **2017**, *118*, 088001.

(35) *Applications of Microporous Glass Membranes: Membrane Emulsification*; Kandori, K., Gaonkar, A., Eds.; Elsevier, 1995; p 113.

DOI: 10.1021/acs.langmuir.7b02048
Langmuir 2017, 33, 12155−12170

(36) Charcosset, C.; Limayem, I.; Fessi, H. The membrane emulsification process—a review. *J. Chem. Technol. Biotechnol.* **2004**, *79*, 209−218.
(37) Joscelyne, S. M.; Trägårdh, G. Membrane emulsification—a literature review. *J. Membr. Sci.* **2000**, *169*, 107−117.
(38) Nakashima, T.; Shimizu, M.; Kukizaki, M. Membrane emulsification by microporous glass. *Key Eng. Mater.* **1992**, *61*−*62*, 513−516.
(39) Newton, R. H.; Haffegee, J. P.; Ho, M. W. Polarized light microscopy of weakly birefringent biological specimens. *J. Microsc.* **1995**, *180*, 127−130.
(40) Holmberg, K. Identification of lyotropic liquid crystalline mesophases. *Handbook of Applied Surface and Colloid Chemistry*; John Wiley & Sons, 2001; Vol. *2*, Chapter 16, pp 299−332.
(41) Denkova, P. S.; Tcholakova, S.; Denkov, N. D.; Danov, K. D.; Campbell, B.; Shawl, C.; Kim, D. Evaluation of the Precision of Drop-Size Determination in Oil/Water Emulsions by Low-Resolution NMR Spectroscopy. *Langmuir* **2004**, *20*, 11402−11413.
(42) Rotenberg, Y.; Boruvka, L.; Neumann, A. W. Determination of surface tension and contact angle from the shapes of axisymmetric fluid interfaces. *J. Colloid Interface Sci.* **1983**, *93*, 169−183.
(43) Hoorfar, M.; Neumann, A. W. Recent progress in axisymmetric drop shape analysis (ADSA). *Adv. Colloid Interface Sci.* **2006**, *121*, 25−49.
(44) Stanimirova, R.; Marinova, K.; Tcholakova, S.; Denkov, N. D.; Stoyanov, S.; Pelan, E. Surface rheology of saponin adsorption layers. *Langmuir* **2011**, *27*, 12486−12498.
(45) Bird, R. B.; Stewart, W. E.; Lightfoot, E. N. *Transport Phenomena, Example 12.1-2*, 2nd ed.; Wiley: New York, 2002; pp 376−378.
(46) Guttman, S.; Sapir, Z.; Schultz, M.; Butenko, A. V.; Ocko, B. M.; Deutsch, M.; Sloutskin, E. How faceted liquid droplets grow tails. *Proc. Natl. Acad. Sci. U.S.A.* **2016**, *113*, 493−496.

DOI: 10.1021/acs.langmuir.7b02048
Langmuir 2017, 33, 12155−12170